SUPPORTING INFORMATION

Smart Assembly of Mn-Ferrites/Silica Core-Shell with Fluorescein and Gold Nanorods: A Robust and Stable Nanomicelle for In Vivo Triple Modality Imaging.

Ilaria Monaco,[a] Paolo Armanetti,[b] Erica Locatelli,[a] Alessandra Flori,[c] Mirko Maturi,[a] Serena Del Turco,[b] Luca Menichetti,[b]* Mauro Comes Franchini [a]*

[a.] Dr. I. Monaco, Dr. E. Locatelli, M. Maturi, Prof. M. Comes Franchini
Department of Industrial Chemistry "Toso Montanari". University of Bologna. Viale Risorgimento 4, 40136 Bologna (Italia)
E-mail: mauro.comesfranchini@unibo.it

[b.] P. Armanetti, S. Del Turco, L. Menichetti
CNR Institute of Clinical Physiology, Via Moruzzi, 1 56124 Pisa (Italia)
E-mail: luca.menichetti@ifc.cnr.it

[c.] A. Flori
CNR /Fondazione Toscana G. Monasterio, Via Moruzzi, 1 56124 Pisa (Italia)

Experimental procedures

Synthesis of HS-PEG-Alkyne

Thiol moiety able to interact with the gold nanorods surface has been introduced in the α-Amino-ω-alkyne PEG chains by using EDC Chemistry to form an amine bond with thioglycolic acid (TGA). α-Amino-ω-alkyne PEG (Mw 3000 g/mol, 0.13 mmol) has been added to 6 mL of ultrapure water at room temperature under magnetic stirring until the complete dissolution. In a different flask thioglycolic acid (0.040 mmol) has been added in a water solution containing N-(3-Dimethylaminopropyl)-N-ethylcarbodiimide hydrochloride (0.040 mmol, EDC), in order to activate the carboxylic group of TGA. After 10 minutes, the activated TGA has been added to the first solution and the reaction has been left under magnetic stirring over night at room temperature.

Then water has been removed under vacuum, the product has been characterized by used without further purification. The product was characterized with H-NMR and FTIR-ATR spectroscopy.

Synthesis of GNRs-Alkyne

GNRs stabilized with the surfactant agent hexadecyltrimethylammonium bromide (GNRs-CTAB) were prepared following the seed mediated grow method reported in literature. [i,ii]

After purification GNRs-CTAB (5 mL) were incubated with a water solution (5 mL) containing α-Mercapto-ω-amino PEG hydrochloride (0.007 mmol) and α-Mercapto-ω-carboxy PEG (0.007 mmol) and the previously synthetized ligand α-Thiol-ω-alkyne PEG (0.013 mmol). The suspension was left under mechanical stirring for 24 h, in order either to form on GNRs surface a moiety able to react with the azide group of $MnFe_2O_4@SiO_2-NH_2/N_3$ completely but also to remove the surfactant CTAB, which is considered extremely cytotoxic. The so-obtained PEGylated GNRs were collected by centrifugation (3 X 6000 RPM, 30 minutes) and dissolved in 5 mL of water. The PEGylated GNRs were completely characterized with ^{1}H-NMR, C-NMR and FTIR-ATR, that showed the CTAB removal (Figure S4).

Synthesis of azide modified 3-aminopropyl)trimethoxysilane (APTMS-N$_3$)

Under nitrogen atmosphere, the (3-Iodopropyl)trimethoxysilane (0.01 mmol) has been dissolved in 5 mL of anhydrous DMF. After that, sodium azide (0.02 mmol) has been added to the solution in order to realize a nucleophilic heterogeneous reaction with the silane precursor. The reaction was left overnight under magnetic stirring at room temperature. Then, anhydrous pentane has been used to extract the formed (azide-propyl)trimethoxysilane from the reaction mixture. 10 mL of anhydrous pentane has been added to the reaction and the suspension was stirred for 3 hours under inert atmosphere.

After that the salts present in the solution, have been removed by filtration on Bucker, in order to collect the solvent. The pentane organic phase, contained in the organic biphasic solution has been separated from the phase constituted by DMF, which has been further washed with anhydrous pentane in order to collect the entire formed product.

After the pentane evaporation, the (azide-propyl)trimethoxysilane has been obtained as pale-yellow oil that was stored at 4°C. The product has been characterized with FTIR-ATR.

Synthesis of fluorescein modified 3-aminopropyl)trimethoxysilane (APTMS-FITC)

Fluorescein 5-isothiocyanate (0.90 mmol) has been dissolved in 20 mL of ethanol under magnetic stirring. Then, (3-Aminopropyl)trimethoxysilane (0.86 mmol) has been added to the formed solution, and the reaction was left over night at room temperature. After that, the ahanol has been evaporated and the fluorescein modified 3-aminopropyl)trimethoxysilane (APTMS-FITC) was used without further purification.

Synthesis of $MnFe_2O_4$

Manganese iron oxide nanoparticles ($MnFe_2O_4$) was synthetized through the thermal decomposition method following procedure reported in literature.[17] Oleic acid (6 mmol), oleyl ammine (6 mmol) and 1,2-hexadecandiol (10 mmol) have been dissolved in benzyl ether (20 mL) under magnetic stirring in nitrogen atmosphere. After that, iron (III) acetylacetonate (2 mmol) and manganese (II) acetylacetonate (1 mmol) have been introduced in the solution. The mixture was heated at 200°C for 2 hours then lead to reflux for 1 hour.

The mixture was then cooled to room temperature. The $MnFe_2O_4$ nanoparticles were purified by magnetic precipitation with excess of cold ethanol, dispersed in 5 mL of hexane, and washed with ethanol. The nanoparticles were redispersed in 5 mL of hexane (15 mg/mL).

Synthesis of fluorescent Core−Shell Manganese Iron Oxide−Silica Nanoparticles ($MnFe_2O_4@SiO_2$-NH_2/N_3/FITC)

The $MnFe_2O_3@SiO_2$-NH_2/N_3/FITC have been synthetized by following a method recently reported in literature.[iii] Briefly, hydrophobic $MnFe_2O_4$ NPs have been encapsulated in hydrosoluble micelles constituted by cetyltrimethylammonium bromide (CTAB). For this purpose, CTAB (1.37 mmol) was dissolved in 25 mL of water and sonicated with a tip-probe sonicator (600 W, 50% amplitude, 6 min) with 2.5 mL of a solution of $MnFe_2O_4$ NPs (60 mg) in hexane. The hexane was then removed from the obtained solution by heating at 70 °C for 10 min under magnetic stirring. The as-synthesized micelles were diluted with 125 mL of water, and 2.5 mL of ethyl acetate and 3.4 mL of a 28% NH_3 solution were added under vigorous stirring. After 10 min, 1.5 mL of MTEOS was added drop-wise, and the mixture was stirred for 3 days at room temperature (25−30 °C). Next, 0.9 mL of 3 aminopropyl-methoxysilane (APTMS), 0.3 mL of APTMS-N_3 and 0.1 mL of APTMS-FTIC were added dropwise, and the mixture was stirred for 3 more days at room temperature.

The $MnFe_2O_4@SiO_2$-NH_2/N_3/FITC NPs were purified by centrifugation (6000 rpm, 1 h) in water. To remove the CTAB, the $MnFe_2O_4@SiO_2$-NH_2/N_3/FITC were stirred for 30 min in a mixture of ethanol and acetic acid (95:5) and centrifuged (6000 rpm, 30 min) three times. Finally, the last purifications were performed by centrifugation in ethanol and water (1:1). The $MnFe_2O_4@SiO_2$-NH_2/N_3/FITC were dispersed in 10 mL of water (5 mg/mL).

MRI relaxivity measurements at 3T

An in-house developed T_2 mapping sequence was used for measuring the transverse (T_2) relaxation time, prescribed as follows: Field of View (FOV) = 16 x 16 cm^2, 224 x 224 matrix, Repetition Time (TR) = 1200 ms, slice thickness = 5 mm, Number of Excitations (NEX) = 2, Echo time (TE) = 7, 14, 21, 28, 35, 42, 49, 57, 64, 71, 78, 85, 92, 99, 106, 113 ms. A Spin Echo Inversion Recovery (IR) sequence was used for longitudinal (T_1) relaxation measurements with the following parameters: FOV = 16 x 16 cm^2, 224 x 224 matrix, TR = 5000 ms, slice thickness = 5 mm, NEX = 2, TE = 8.5 ms, Inversion Time (TI) = 50, 100, 300, 450, 600, 900, 1100, 1200, 1300, 1500, 1700, 2000, 2400 ms.

Post-processing of the MRI data was conducted in Matlab (The MathWorks Inc., Natick, MA, USA). Regions-of-interest (ROIs) were selected on MRI images for each nanoparticles concentration values, and the corresponding average signal was determined.

For IR acquisitions, the average MR signal was reported as a function of TI and the T_1 relaxation time was obtained from the fit of the curve, according to:

$$M = M_0(1 - 2 * e^{-TI/T_1})$$

where M stands for the magnetization signal and M_0 is the equilibrium magnetization.

Conversely, T_2 was determined by fitting the curve obtained by reporting the average MR signal in the ROI as a function of TE and using the following equation:

$$M = M_0 * e^{-TE/T_2}$$

The relaxation rates $R_{1,2}$ were then calculated as the inverse of the relaxation times $T_{1,2}$ for each nanoparticles solution. To provide a semi-quantitative evaluation of the nanoparticles -induced relaxation effect, the longitudinal (r_1) and transverse (r_2) relaxivities were estimated from the slope of the best-fit line between $R_{1,2}$ and nanoparticles concentration (expressed in mM Fe^{3+} concentration).[iv]

Phantom and ex vivo fluorescence tests

The fluorescence intensity of the nanoparticles containing fluorescein (excitation, and emission wavelengths were 495 and 519 nm, respectively) was measured by Photon ImagerTm (PIT) product by Biospace Lab. detection. The tests of localization and quantification of dynamic optical signal were carried out in PE tube and in ex-vivo model. A PE tube was loaded with around 30μL and the fluorescence was calculated acquiring an image of 966 x 750 pixels. The sample of chicken breast was injected with a bolus of 10μL of $MnFe_2O_4@SiO_2@GNRs@PMs$ using the same previous parameters.

In vitro **haemolysis test**

To assess the effect of nanoparticles on erythrocyte integrity, hemolysis test was performed by spectrophotometric measurement of hemoglobin release, after erythrocyte lysis. 0.2 mL of NP suspension at different concentrations (5-50-500 μg/mL) diluted in PBS, were added to 0.8 mL of sodium-citrate whole blood from healthy volunteers and incubated at 37°C for 1, 2 and 4 h at constant vortexing. Then, plasma was separated by centrifugation at 1000 g for 10 min and optical density of the supernatant was measured at 540 nm in a plate reader. Control samples were prepared incubating whole blood with PBS, without NP suspension, at the ratio corresponding to NP sample dilution. Data are expressed in arbitrary units of absorbance (AU) (mean ± SD, n=3). Sample absorbance was corrected for background interference due to NP suspension in PBS without blood.

Photoacoustic Acquisitions

The photostability (PHS) and the spectroscopic PA analysis (SPA) were studied to characterize the PA behavior of $MnFe_2O_4@SiO_2@GNRs@PMs$. The PA values were calculated into selected regions of interest (ROI), drawn by software tool, on the PA images acquired. For each acquisition, the dataset of PA signals was obtained from ROIs of the same size. The SPA was performed studying the spectral PA response of the sample, using a laser stimulation of 146 wavelengths (step 2 nm) in the range between 680 and 970 nm, at 26 mJ of maximum energy peak. The PHS was evaluated over 1 minute (335 laser shots) under pulsed irradiation at 730 nm and 800 nm respectively for in vitro and ex vivo tests. The average of PA signals and their relative standard deviations σ were calculated on average of 335 points. The PA signal is proportional to the absorbance spectrum, that was acquired by a spectrophotometer (Tecan infinite 200 PRO) for all dilutions and the linear relation between concentration and absorption was checked. The linear relation between PA signal and concentration was verified by linear fitting of values obtained from the PHS acquisitions. By this method, the *sensitivity* was extrapolated and the *MDC* calculated by the following equation:

$$MDC = \frac{\sum_{1}^{i} \sigma_i}{S}$$

Where the *sensitivity (S)* was obtained from the slope of the calibration curve (IUPAC) and σ_i are the standard deviations of each acquired point during the PHS measurement. The PA gain losses for each concentration of $MnFe_2O_4@SiO_2@GNRs@PMs$ during time, due to the laser irradiation, were assessed with the percentage difference between the data acquired at the first and last 3 seconds of PHS acquisitions. In this work, the quality of acquisition was improved, coupling the PA probe with water; by this way, the ultrasonic path and the region between the probe and the sample was air bubbles free. Post processing, into the PA images acquired from the in vitro tests, testing region was drawn around the section of each tube filled with a different dilution of $MnFe_2O_4@SiO_2@GNRs@PMs$ and another one drowns around the MC tube, that it was used as background PA estimation. The in vivo / ex vivo study were performed acquiring the PAS from the left leg in basal condition and after the subcutaneous injection of 100μL of $MnFe_2O_4@SiO_2@GNRs@PMs$ stock solution. During the in vivo test, the PHS at 710 nm was studied and SPA extrapolated. The contrast to noise ratio (*CNR*) and the contrast (C) were employed as image quality parameters and estimated according to the following equations:

$$CNR = \frac{Signal - background}{\sqrt{\sigma_s^2 + \sigma_b^2}} \quad ; \quad C = \frac{Signal - background}{background}$$

(5)

Where Signal and background are the average of acquired signals, σs and σb their standard deviations calculated in the regions of interest in the PA images. Finally, the mouse was sacrificed and the injected region was surgically resected to study more finely the distribution of $MnFe_2O_4@SiO_2@GNRs@PMs$ in this sample section.

Chemophysical Characteristics of the nanosystems
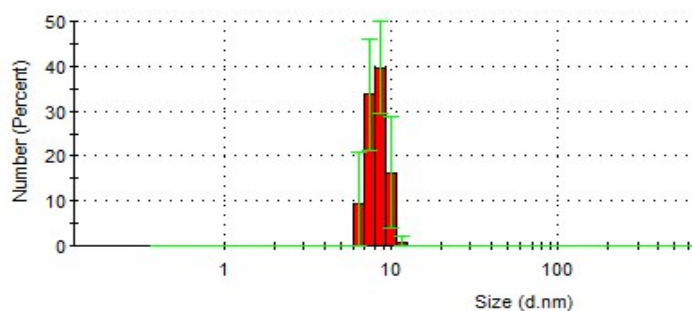
Figure S1.Dynamic light scattering (DLS) results of $MnFe_2O_4$ nanoparticles in hexane.
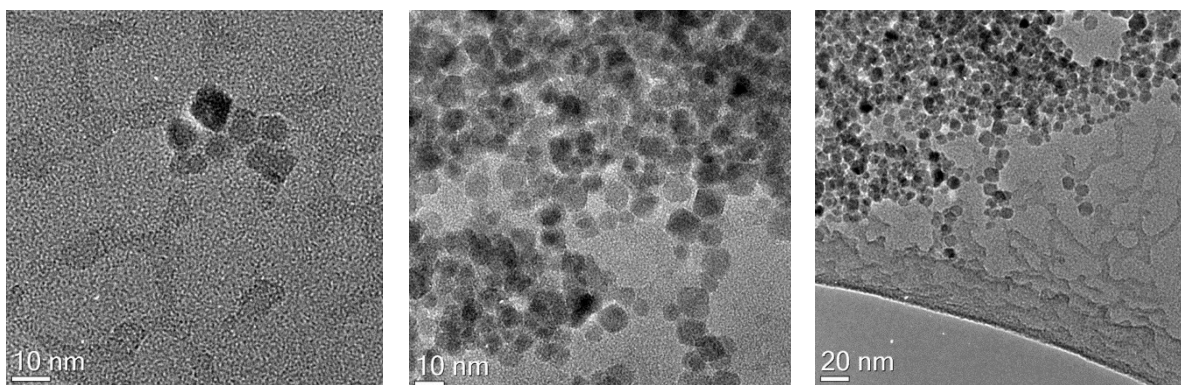
Figure S2. TEM images of $MnFe_2O_4$ nanoparticles

Element	Weight %	Uncert. %	Atomic %
O (K)	32.95	1.15	63.11
Mn (K)	12.06	0.44	6.72
Fe (K)	54.97	1.00	30.15

Table S1. EDX analysis of $MnFe_2O_4$ nanoparticles
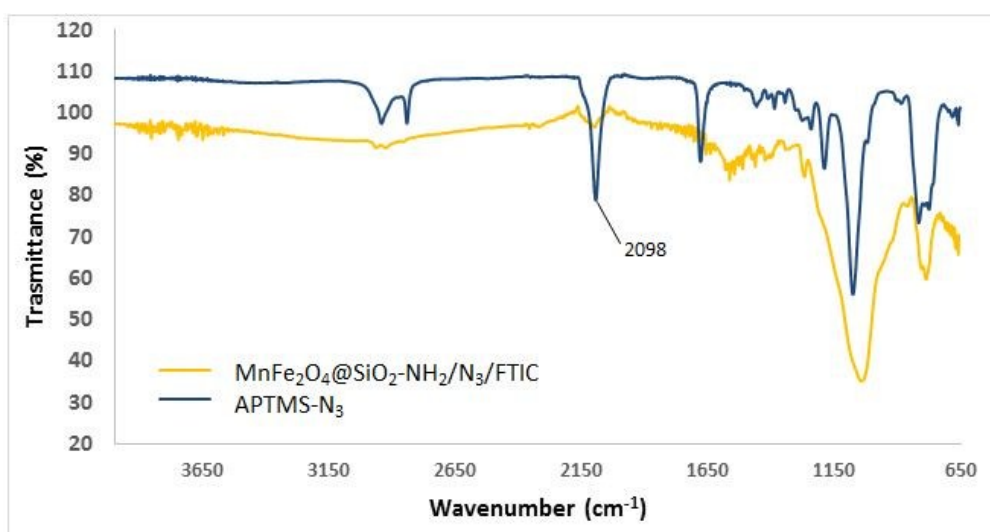
Figure S3. FT-IR analysis of $MnFe_2O_4@SiO_2$-NH_2/N_3/FTIC nanoparticles . The graph show the typical peak at 2098 cm^{-1} of the azide group in the synthetized APTMS-N_3 (Blu line), that is present also on $MnFe_2O_4@SiO_2$-NH_2/N_3/FTIC nanoparticles surface (Yellow Line).
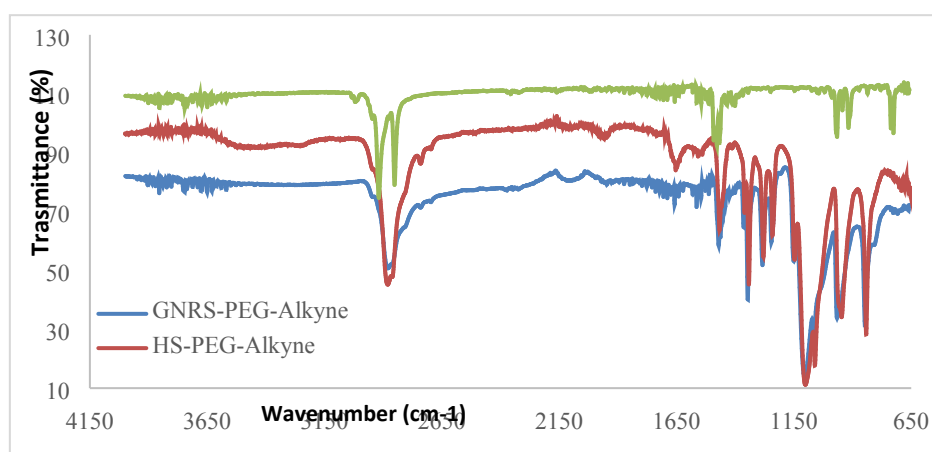
Figure S4. FT-IR analysis of ligand exchange reaction on GNRs.
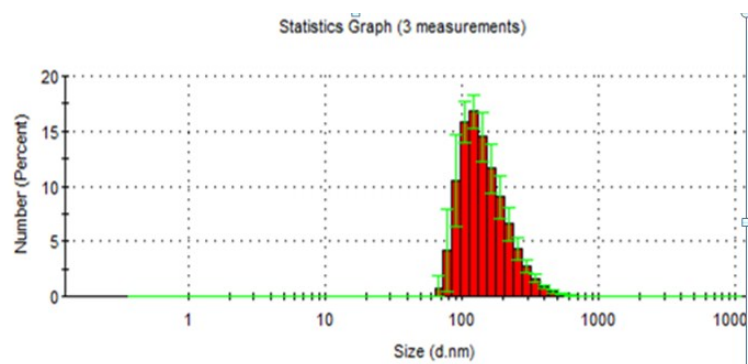
Figure S5. Dynamic light scattering (DLS) results of $MnFe_2O_4@SiO_2$-NH_2/N_3/FTIC nanoparticles in water.
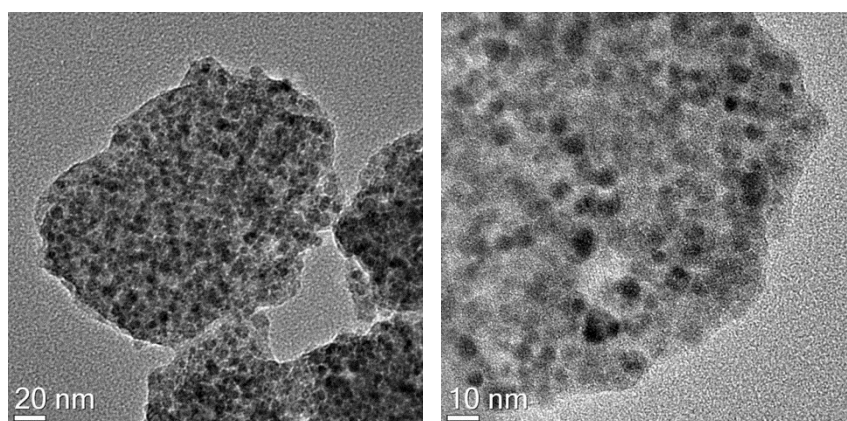
Figure S6. TEM images of $MnFe_2O_4@SiO_2$-NH_2/N_3/FTIC nanoparticles
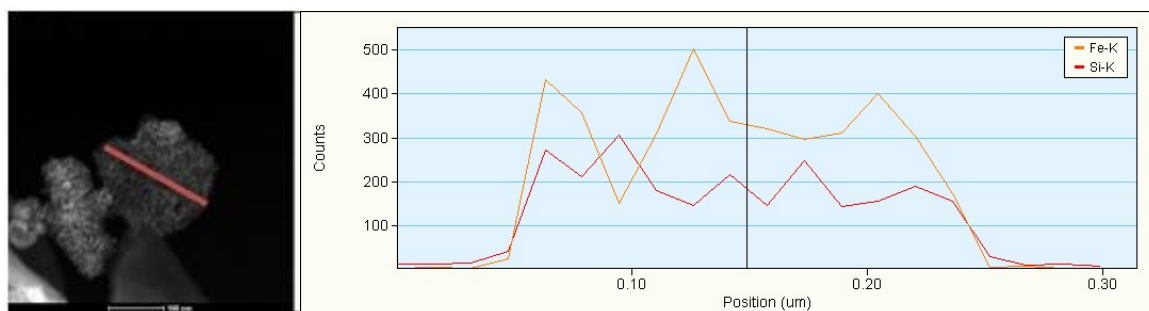
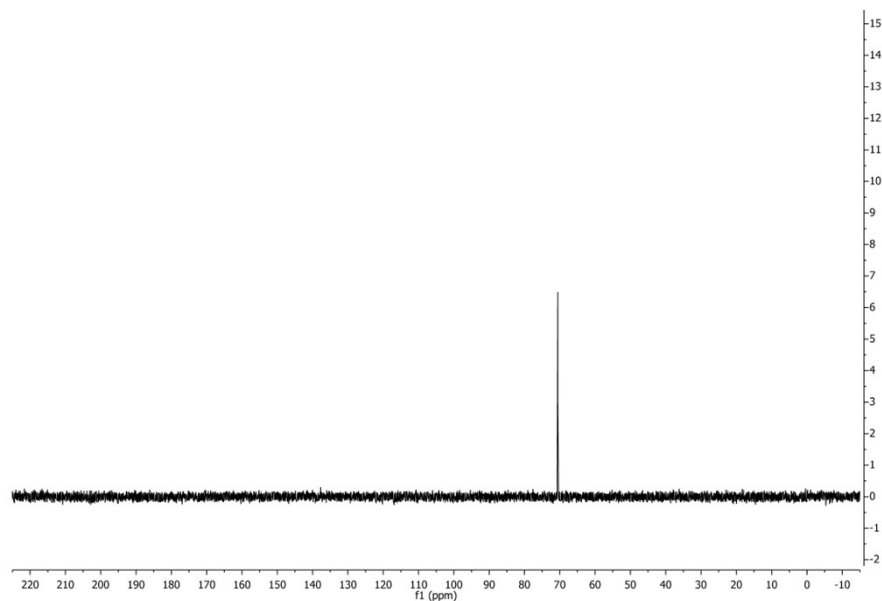**Figure S7**. EXD analysis of $MnFe_2O_4@SiO_2$-NH_2/N_3/FTIC nanoparticles

Figure S8. ^{13}C-NMR DEPT *(distortionless enhancement f polarisation transfer)* spectrum of PEGylated-GNRs showing only the tertiary carbon of acetylene ($^{-}$C≡**C**H).

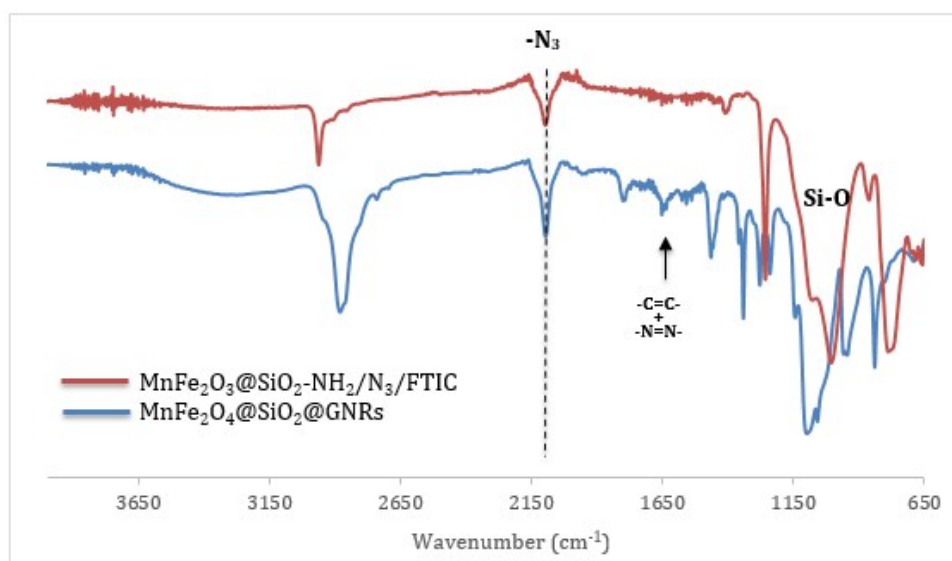**Figure S9**. FT-IR spectroscopy of MnFe$_2$O$_3$@SiO$_2$-NH$_2$/N$_3$/FTIC and MnFe$_2$O$_4$@SiO$_2$@GNRs nanoparticles
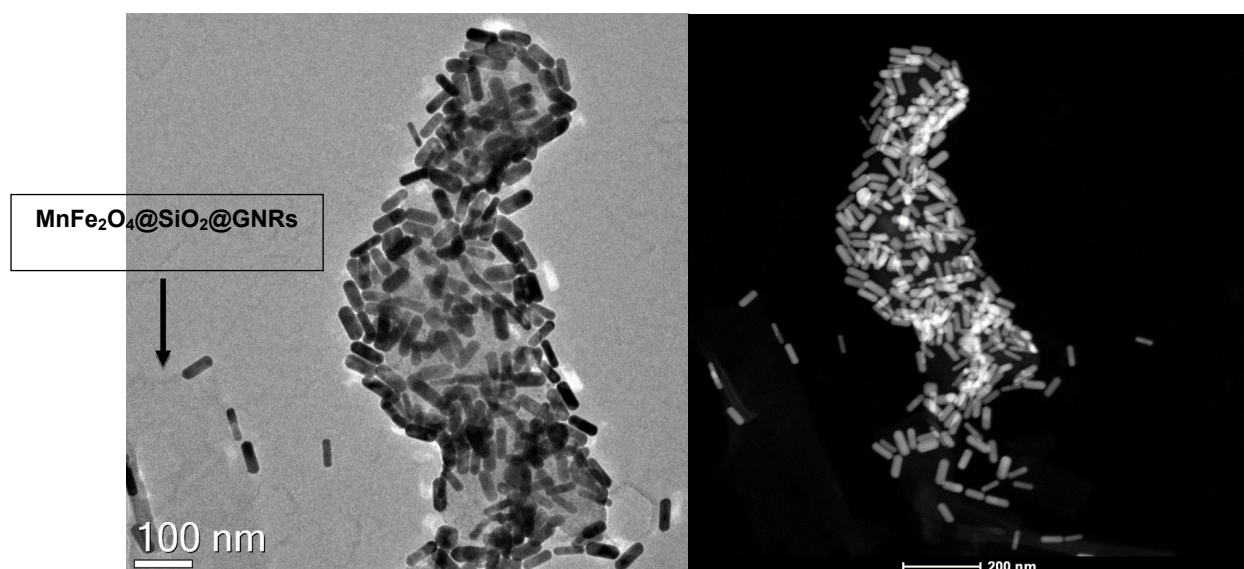
Figure S10. TEM and STEM-HAADF images of MnFe₂O₄@SiO₂@GNRs nanoparticles
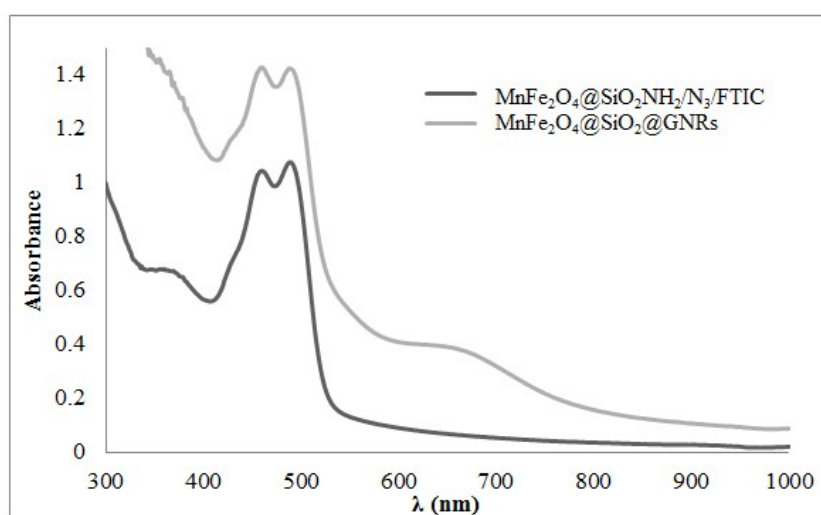
Figure S11. UV-Vis analysis of MnFe₂O₄@SiO₂@GNRs
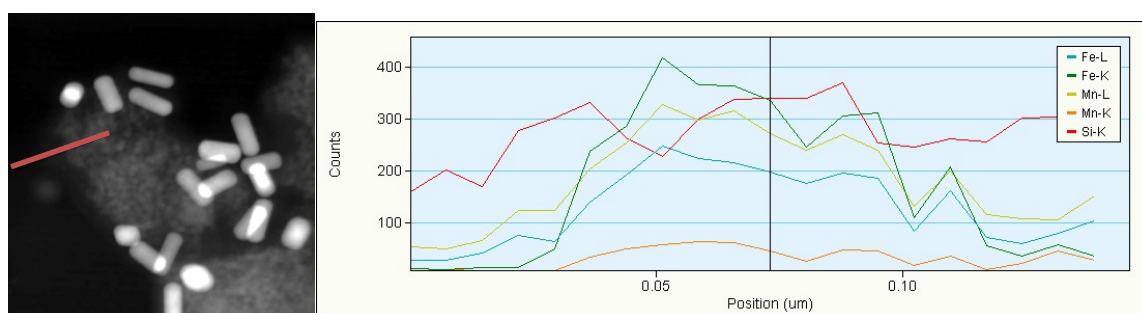
Figure S12. EXD analysis of MnFe₂O₄@SiO₂@GNRs nanoparticles
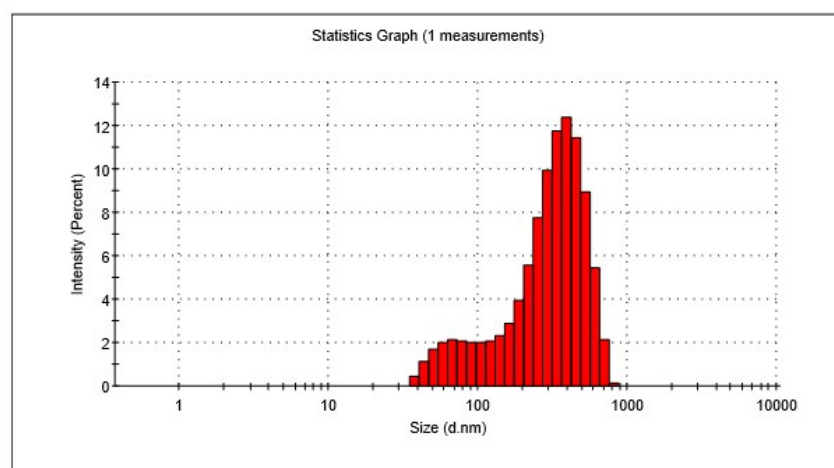
Figure S13. Dynamic light scattering (DLS) results of $MnFe_2O_4@SiO_2@GNRs@PMs$ nanomicelles in water.

$MnFe_2O_4@SiO_2@GNRs@PMs$	Size (nm)		Zpot (mV)	
	0 h	48 h	0 h	48 h
H2O uup	376.6 ± 7.4	388.1 ± 9.1	-13.5	-11.2
PBS Buffer (pH = 7.4)	381.3 ± 8.1	395.7 ± 6.5	- 8.2	- 7.8
Serum	393.1 ± 3.4	399.4 ± 9.0	- 2.5	- 3.7

Table S2. Dynamic light scattering (DLS) characterizations of the $MnFe_2O_4@SiO_2@GNRs@PMs$ in different aqueous environment after the synthesis and after 48 hours.

MRI relaxivity measurements at 3T

As previously demonstrated[v], the Mn content of paramagnetic nanoparticles could reduce the T_1 relaxation time, leading to a positive MRI contrast. In particular, the nanoparticles size can be suitably tailored to exert either negative or positive contrast effect, for which a smaller size (of the order of 5 nm) favors a T_1-dominated contrast. Although the positive contrast capability of these systems was not comprehensively investigated here, we reported the R_1 values as a function of Mn concentration

and we found an increase of the r_1 relaxivity for $MnFe_2O_4@SiO_2$-NH_2/N_3@PMs with respect to $MnFe_2O_4@SiO_2$-NH_2/N_3. Moreover, the r_1 relaxivity was further increased after GNRs binding.

This new type of contrast agents might become a new generation of multimodal systems, potentially able to overcome the intrinsic limitations of pure T_2-weighted contrast agents and the nephrotoxicity of conventional gadolinium-based T_1 contrast agents. Moreover, the intrinsic multimodality of $MnFe_2O_4@SiO_2@GNRs$ nanoparticles could realise *in practice* the integration of bio-imaging tools and theranostic agents.

Taken together, the data recorded in this study suggest a major efficacy of the proposed nanoparticles as negative T_2-contrast agents and multi-modal imaging platform, suitable for potential *in vivo* diagnostic applications. The strategies for the application of $MnFe_2O_4@SiO_2@GNRs@PMs$ as T_2 and T_1 imaging agents go through an enhancement of the r_1 values of the $MnFe_2O_4$ core, for instance by improving the crystallinity, particle size, and/or morphologies.

Further challenges may deal with surface modifications to prolong the short retention time due to the large size as well as the implementation of active targeting strategies or cell-based targeting to modify the nanoparticles extraction in the pathological lesions.

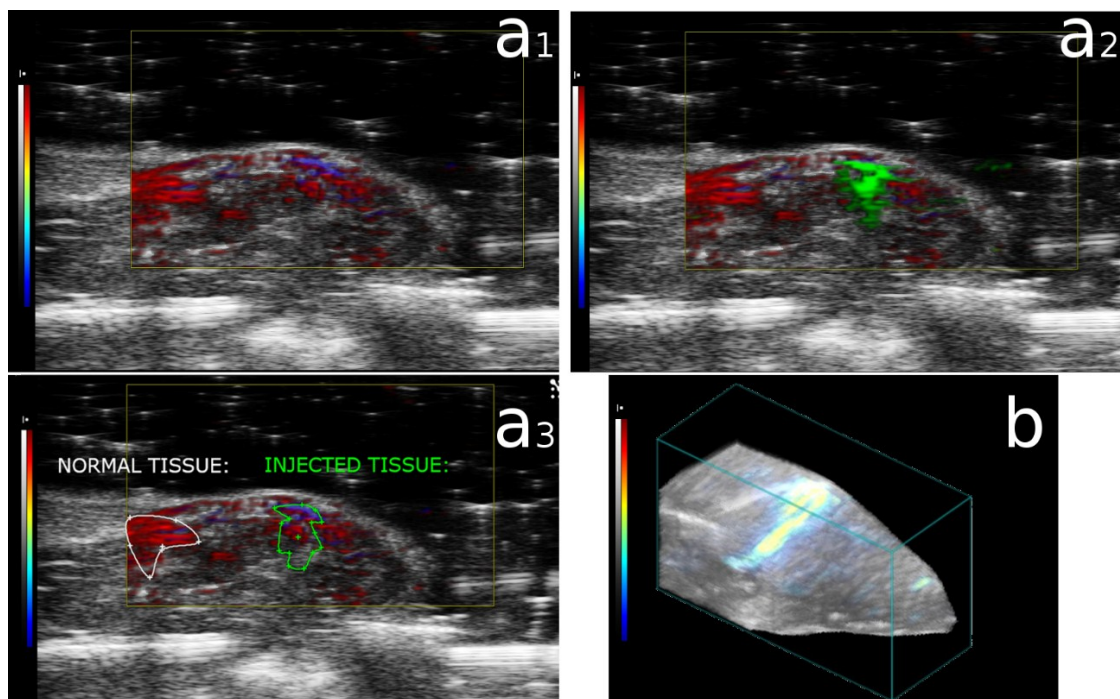**Spectral *unmixing* for nanostructures tracking**

Figure S14: Spectral Unmixing Analysis: (a1),(a2),(a3), PA images processed with spectral unmixing control: in the first one was discriminated the spectral response of oxy and deoxy hemoglobin, in the second one, the previous spectral responses with the discrimination and localization of $MnFe_2O_4@SiO_2@GNRs@PMs$ perfusion inside the same region, the last one, semi quantitative analysis in two ROIs in which were evaluated the sO2, the Hbt and the PA signal weighted for each different spectral contribute; (b) 3D render of PA distribution of $MnFe_2O_4@SiO_2@GNRs@PMs$ into the tissue of biological sample.

We performed spectral unmixing analysis to evaluate and distinguish the spectral contributes of different molecular patterns. As shows in Figure $S10a_{1,2,3}$, the deoxygenayted (blue scale)/oxygenated (red scale) hemoglobin and the $MnFe_2O_4@SiO_2@GNRs@PMs$ (green scale) spectra were processed by the unmixing algorithm, that were differentiated and spatially localized into the image without overlapping (Figure $S10(a_{1,2})$). The PA unmixing analysis provided a semi quantitative evaluation of haemoglobin oxygen saturation (sO_2), the total number of hemoglobin (Hbt) and the amount of the PA response produced by the three components (Figure $S10(a_3)$), that were related to their concentrations in the selected region (injected and *non-injected*). At least, in Fig. 9b there are the 3D render of photoacoustic distribution of $MnFe_2O_4@SiO_2@GNRs@PMs$ inside the chicken breast sample. The results of semiquantitative analysis (Table S7) confirm the clear discrimination of

different PA responses in the selected ROIs by using the molecular fingherprint of MnFe$_2$O$_4$@SiO$_2$@GNRs@PMs.

Photoacoustic Data

	Impedance (kRayl)	Sound Speed(m/s)	Density (g/cm3)
Soft Tissues	~1,64	~1540	~1,0
Water (37°C)	~1,48	~1520	~0,99
Agar	~1,57	~1500	~1,04
Polyethylene	~1,73	~1950	~1,73
Polypropilene	~2,40	~2740	~0,88

Table S3: Physical properties of material used for phantom preparation

Concentration	Mean Value	Std.Dev.	CNR		CONTRAST		PHS (a.u. · min^{-1})
			Mean	3s	Mean	3s	
1:4	6.4	0.2	31	46	38	36	±3%
1:8	3.0	0.1	29	37	17	17	±1.7%
1:16	1.87	0.06	27	16	10	11	±6%
1:32	0.69	0.03	18	14	3	3	±2.3%
Sensitivity	27±3						
MDC	0.014						

Table S4: Photoacoustic *in vitro* results, the values CNR and Contrast were calculated by averaging on the total irradiation time (mean) and in the first 3s of irradiation (3s)

Linear Regression for PAS vs Concentration

	PAS = Sensitivity * Concentration + q

Coefficient	Value	Error
q	-0,29	0,18
Sensitivity	27	3

R	SD	#Points	Pearson
0,98518	4,69168	4	0,01482

Table S5: schematic of linear regression PAS *vs* Concentration

Concentration	Mean Value	Std.Dev.	CNR		CONTRAST		PHS (a.u. · min⁻¹)
			Mean	3s	Mean	3s	
1:2	*1,96*	*0,04*	*48*	70	*17*	17	±3%
1:5	*1,71*	*0,04*	*39*	37	*15*	16	±1.7%
1:8	*1,86*	*0,04*	*45*	44	*14*	15	±6%
1:10	*0,707*	*0,006*	*14*	52	*5*	6	±2.3%

Table S6: Photoacoustic *ex vivo* results, the values *CNR* and *Contrast* were calculated by averaging on the total irradiation time (mean) and in the first 3s of irradiation (3s)

Concentration	Mean Value	Std.Dev.	CNR		CONTRAST		PHS (a.u. · min⁻¹)
			Mean	3s	Mean	3s	
Stock solution	*2,42*	*0,03*	*60*	64	*8*	8	±1,5

Table S7: Photoacoustic results, the values *CNR* and *Contrast* were calculated by averaging on the total irradiation time (mean) and in the first 3s of irradiation (3s)

| ROI | Area (mm²) | PA Value | | | %sO₂ |
		GNRs	DeOxy	Oxy	
Normal tissue	4,499	0,062	0,079	0,368	82,561
Injected tissue	3,785	0,795	0,193	0,279	60,906

Table S8: Spectral unmixing analysis: discrimination of different molecules and semiquantification of oxygen saturation (sO2) and total hemoglobin (Hbt)
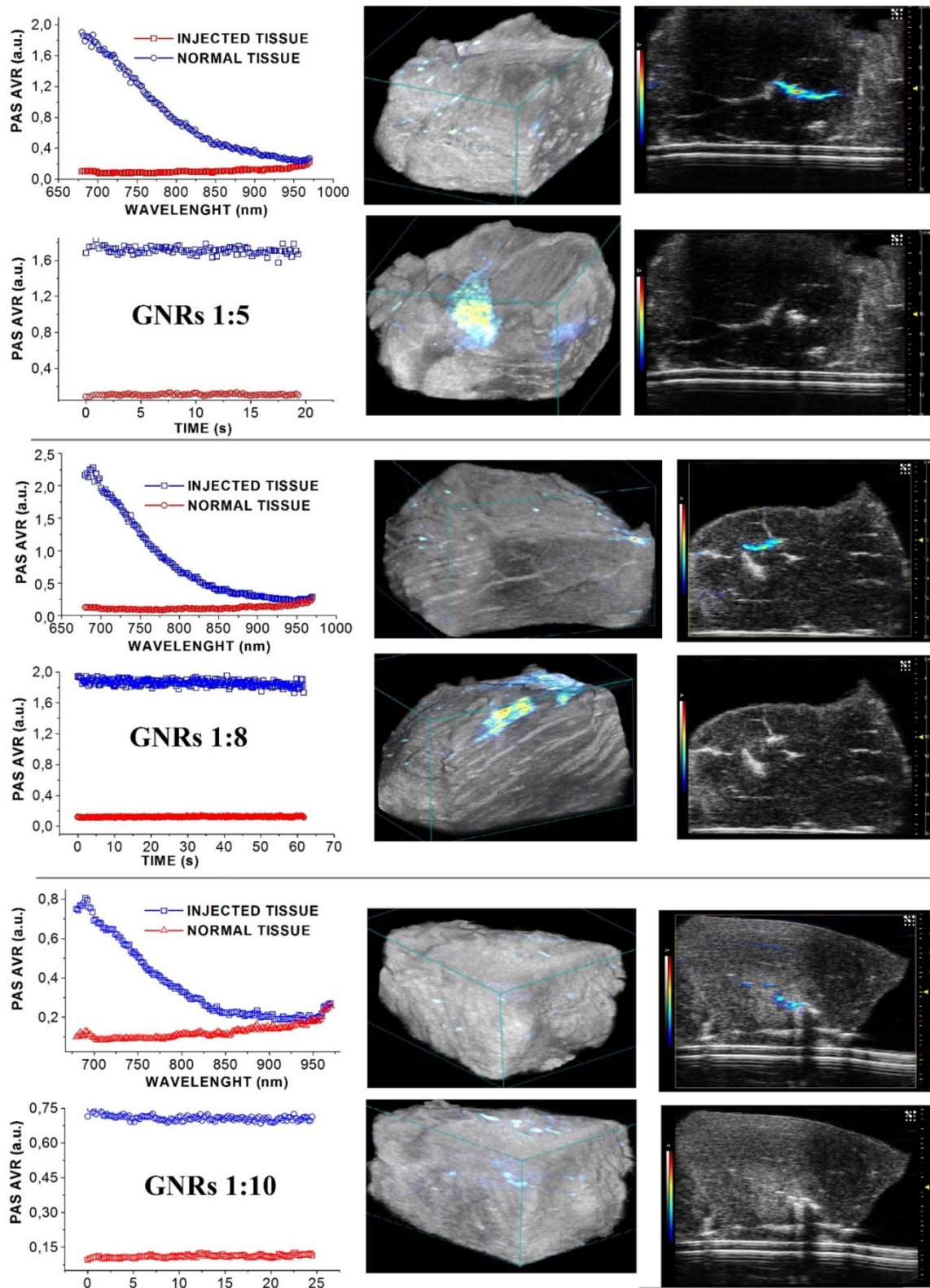
Figure S15: PA test *ex vivo*: SPA and PHS for 1:5, 1:8, 1:10 dilution (1° column), 3D PA render of sample in basal condition (up) and after injection (down) (2° column), the PA distribution is drown in rainbow scale; 2D slice of injected region, Pa (up) and Echographic (down) images (3° column)
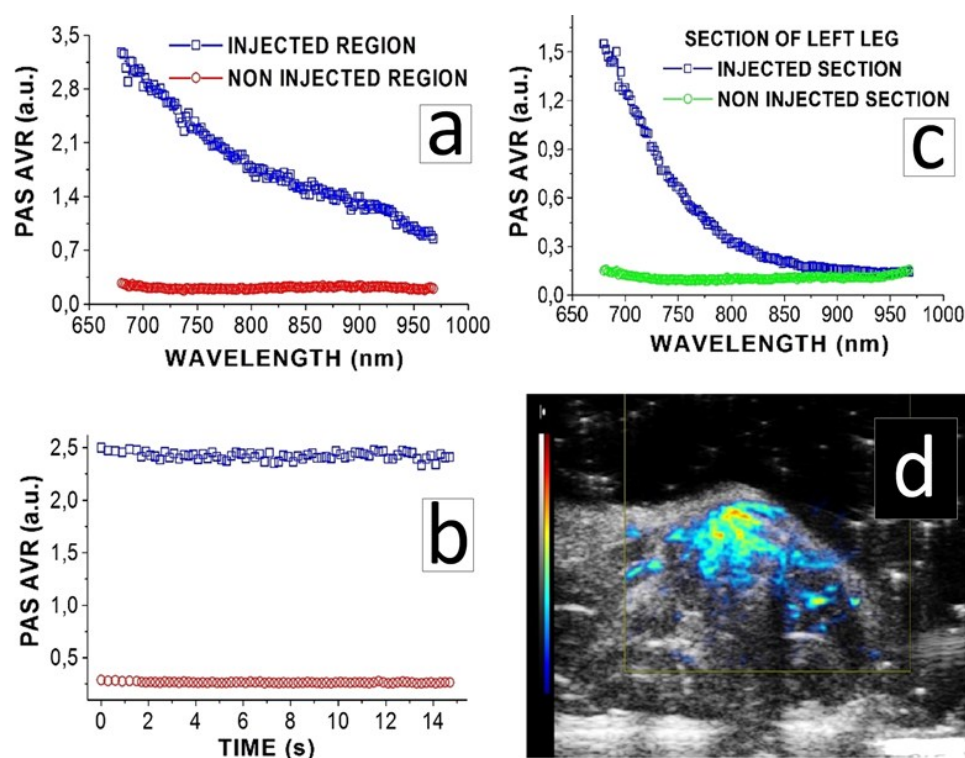
Figure S16: (a), (b) SPA and PHS of injected mouse leg during *ex vivo* test; (c) SPA *ex vivo* of harvested sample of injected mouse leg; (d) 2D PA in vivo image of NPs perfusion in the mouse leg.

Concentration of NPs	Optical density (OD, mU)
0 μg/mL	65±6
5 μg/mL	64±4
50 μg/mL	63±2
500 μg/mL	67±4

OD mU: milliunits of optical density

Table S9. Hemolytic activity of NPs

References

[i] B. Nikoobakht, M.A. El-Sayed, Chem. Mater., **2003**, 15, 1957–1960.

[ii] C. J. Murphy, T. K. Sau, A. M. Gole, C. J. Orendorff, J. Gao, L. Gou, S. E. Hunyadi, T. Li, J. Phys. Chem. B, **2005**, 109, 13857–13870.

[iii] I. Monaco, F. Arena, S. Biffi, E. Locatelli, B. Bortot, F. La Cava, G. M. Marini, G. M. Severini, E. Terreno, M. Comes Franchini; Bioconjugate Chem. **2017**, 28, 1382−1390.

[iv] Laurent et al. Chem. Rev. 2008, 108, 2064–2110, 10.1021/cr068445e

[v] Huang et al. Nanoscale, 2014, 6, 10404-10412, DOI: 10.1039/c4nr02680b